Stable Scatterers Detection and Tracking in Heterogeneous Clutter by Repeat-Pass SAR Interferometry.

Andrei Anghel, Gabriel Vasile
Grenoble-Image-sPeach-Signal-Automatics Lab, CNRS / Grenoble-INP, FRANCE

Jean-Philippe Ovarlez
ONERA, FRANCE

Guy d'Urso, Didier Boldo
EDF R&D, STEP, FRANCE

Abstract

This paper presents a novel strategy for Stable Scatterers detection and tracking by repeat-pass SAR interferometry by coupling sub-band / sub-aperture decomposition prior to the GLRT-LQ detector. The proposed method is tested with spaceborne InSAR images provided by the TerraSAR-X satellite.

1 Introduction

The multiplicative model has been employed for SAR data processing as a product between the square root of a scalar positive quantity (texture) and the description of an equivalent homogeneous surface (speckle) [1]. For an m-dimensional repeat-pass SAR interferometry (InSAR) system, the single channel model [2] has been extended as follows. In each azimuth / range location, let $\mathbf{k}$ be the $m \times 1$ complex target vector corresponding to the same area on the ground. Recent studies [3] show that the higher scene heterogeneity induced by the high-resolution spaceborne SAR systems (TerraSAR-X, TanDEM-X, COSMO-SkyMed, SAR-Lupe...) leads to non-Gaussian interferometric clutter modeling.

In the case of conventional InSAR system two channels are involved and $m = 2$. Denoting by $c = \rho \exp(j\phi)$ the complex correlation coefficient, the target relative displacement d_{12} between the two acquisitions can be retrieved from the exact knowledge of SAR antenna phase center positions, terrain height, acquisition geometry, and an estimate of the differential interferometric phase ϕ_{12} . ρ_{12} is called interferometric coherence and it describes the phase stability within the estimation neighborhood. The phase information ϕ_{12} allows phase differences (interferograms) to be computed in order to measure topography or target displacements between repeated pass acquisitions.

In the general case, the m-dimensional interferometric target vector will contain information about the $m \times m$ relative displacements between each combination of 2 passes. The main parameter to estimate is the speckle covariance matrix, from which normalized correlation coefficients can be derived. Recently, a novel parameter estimation technique has been proposed in this framework [4].

2 Stable Scatterers detection

This section focuses on the analysis of a subset of scatterers within the scene, the so-called Stable Scatterers (SS), characterized by a deterministic point-like scattering behavior. The advantage of SS is that it is widely unaffected by multiple scattering effects and geometrical distortions allowing, as far as possible, a direct interpretation in terms of its phase center displacement. A similar approach has been proposed by the so-called Permanent Scatterers (PS) in SAR interferometry [5], where the identification of PS is based on its temporal stability (coherence over time) and relies on the availability of large time series of SAR image acquisitions. The SS differs from the PS in the sense that there is no need of temporal stability involved in its detection. The usual way to detect SS is to use Time-Frequency Distributions (Short Time Fourier Transform, Wavelet, etc) to form different sub-apertures (sub-looks) or sub-bands of the same scene and to exploit their mutual correlations or coherence.

2.1 Sub-band / sub-apertures decomposition

When a target is illuminated by a broad-band signal and/or for a large angular extent, it is realistic to consider that the amplitude spatial repartition $I(\vec{r})$ of the scatterers depends on frequency f and on aspect angle θ. This repartition, denoted $I(\vec{r}, \vec{k})$, is depending on the wave vector $\vec{k}$ and it represents the energy distribution of the backscattering coef-

ficient $H(\vec{k})$ in the hyperplane $(\vec{r},\vec{k})$. Rewriting $I(\vec{r},\vec{k})$ as $I(x,y,f,\theta)$, one can show that for each frequency f_0 and each angle of radar illumination θ_0, $I(x,y,f_0,\theta_0)$ represents a spatial distribution of the backscattered energy for this frequency [6]. It characterizes an "extended image" relative to the spatial repartition $I(\vec{r})$. Such images can be built using the Short Time Fourier transform (STFT) and are called hyper-images [7]. Since the STFT is an atomic decomposition, the phase of hyper-image is preserved and it can be used for interferometric processing. Moreover, this technique decomposes the SLC signal into 2-D subspectra that can be interpreted as frequency sub-bands and angular sub-sectors (sub-apertures).
Consequently, the SS target with one SAR image can be reformulated in terms of hyper-image concept as a particular target (e.g. corner reflector) exhibiting a "stable" phase signal within all sub-bands / sub-apertures: given the m-dimensional complex target vector formed by m coherent sub-bands / sub-apertures, the SS can be described as the product between the reference signal $\mathbf{p} = [1...1]^T$ (target steering vector) times an unknown scalar complex parameter α (target complex amplitude).

2.2 Binary hypothesis test

In this paper we propose the application of the estimation scheme presented in [8] to Stable Scatterers detection in high resolution SAR images. The SS target detection problem in compound-Gaussian clutter can be formulated as a binary hypothesis test shown in (1). Under the null hypothesis H_0, the observed target vector $\mathbf{k}$ is only the clutter $\mathbf{c}$. Under the alternative hypothesis H_1, the backscattered signal can be decomposed as the sum of the target complex signal with the clutter $\mathbf{c}$. Here, the clutter is modeled as a Spherically Invariant Random Vector (SIRV).

$$\begin{cases} H_0 : \mathbf{k} = \mathbf{c} \\ H_1 : \mathbf{k} = \alpha\mathbf{p} + \mathbf{c} \end{cases} \quad (1)$$

The optimal detector under the SIRV hypothesis is given by the following relation:

$$\Lambda([M]) = \frac{p_{\mathbf{k}}(\mathbf{k}/H_1)}{p_{\mathbf{k}}(\mathbf{k}/H_0)} = \frac{h_p\left((\mathbf{k}-\mathbf{p})^H[M]^{-1}(\mathbf{k}-\mathbf{p})\right)}{h_p\left(\mathbf{k}^H[M]^{-1}\mathbf{k}\right)} \underset{H_0}{\overset{H_1}{\gtrless}} \lambda.$$

where $h_p(\cdot)$ is the density generator function. Its expression is given by:

$$h_p(x) = \int_0^{+\infty} \frac{1}{\tau^p} \exp\left(-\frac{x}{\tau}\right) p_\tau(\tau)\, d\tau.$$

This optimal detector depends on the texture probability density function p_τ.

2.3 GLRT-LQ detector

The Generalized Likelihood Ratio Test - Linear Quadratic (GLRT-LQ) detector can be used to detect a particular target. Let $\mathbf{p}$ be a steering vector and $\mathbf{k}$ the observed signal. The GLRT-LQ between $\mathbf{p}$ and $\mathbf{k}$ is given by [9]:

$$\Lambda([M]) = \frac{|\mathbf{p}^H[M]^{-1}\mathbf{k}|^2}{(\mathbf{p}^H[M]^{-1}\mathbf{p})(\mathbf{k}^H[M]^{-1}\mathbf{k})} \underset{H_0}{\overset{H_1}{\gtrless}} \lambda, \quad (2)$$

where $[M]$ is the covariance matrix of the population under the null hypothesis H_0, *i.e.* the observed signal is only the clutter.
In general, the covariance matrix is unknown. One solution consists in estimating the covariance matrix $[M]$ by $[\hat{M}]_{FP}$, the fixed point covariance matrix estimator [4]. Replacing $[M]$ by $[\hat{M}]_{FP}$ in (2) leads to an adaptive version of the GLRT-LQ detector.The adaptive GLRT-LQ assumes knowledge of the clutter covariance matrix and does not require any "a priori" information about the texture PDF. This detector is also reported to present the Constant False Alarm Rate (CFAR) property with respect to the texture statistical characterization, meaning that the GLRT-LQ probability of false alarm is the same for any texture statistics [10].
If the covariance matrix is estimated by the fixed point estimator, it has been proved, for large N, the relation between the false alarm probability p_{fa} and the detection threshold λ:

$$p_{fa} = (1-\lambda)^{(a-1)}\ {}_2F_1(a, a-1; b-1; \lambda), \quad (3)$$

with $a = \frac{p}{p+1}N - p + 2$ and $b = \frac{p}{p+1}N + 2$. N is the number of pixels used to estimate the covariance matrix $[M]$. p is the dimension of the target vector ($p = 3$ for the monostatic case). ${}_2F_1(\cdot,\cdot;\cdot;\cdot)$ is the Gauss hypergeometric function.
It is important to notice that the maximum likelihood estimator of the target amplitude $\widehat{\alpha}_{ML}$ has been also derived as:

$$\widehat{\alpha}_{ML} = \frac{\mathbf{p}^\dagger[M]^{-1}\mathbf{k}}{\mathbf{p}^\dagger[M]^{-1}\mathbf{p}}. \quad (4)$$

This parameter can be used to obtain energetic information about the target previously detected by the GLRT-LQ.

3 Stable Scatterers tracking

The relative displacement between two stable scatterers from one SLC image to another can be obtained by means of differential interferometry. The positions in the SLC images of the two scatterers are determined by employing the procedure described in the previous section. Fig. 1 shows the geometric configuration of the satellites and the SS targets (points P and Q) for two acquisitions. Points SM and SS show the positions of the satellite when acquiring the master and respectively the slave image. For each pixel in the SAR interferogram obtained from the two images, the phase difference $\Delta\phi_{i,j}$ can be written as:

$$\Delta\phi = \phi_{orbital} + \phi_{topo} + \phi_{disp} + \phi_{atm} + \phi_{noise}, \quad (5)$$

where each term is a partial contribution to the total temporal phase difference.

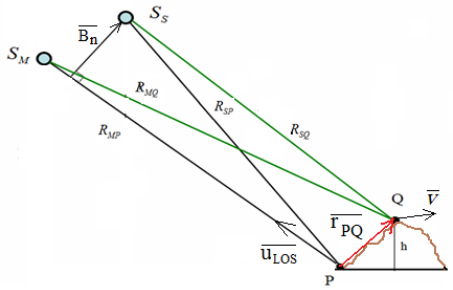

Figure 1: Interferometric tracking geometry.

In order to compute the displacement in Line Of Sight (LOS) of point Q (the mobile SS target) with respect to the reference point P (the fixed target) an additional spatial phase difference is done (between the temporal phase differences of the pixels containing the two targets). After this double phase difference, by using stable scatterers, and assuming same atmospheric conditions for neighboring points, the terms regarding the noise and the atmospheric effects are cancelled. The remaining phase difference $\Delta(\Delta\phi)$ contains two terms: one regarding the orbital and topographic differences and one provided by the displacement in LOS. The first term is given by the satellite?s orthogonal baseline B_n and the distance between the two targets (the "ground" baseline r_{PQ}). The relative displacement in LOS can be computed as in [11]:

$$D_{LOS} \simeq \frac{\lambda}{4\pi}\Delta(\Delta\phi) - \frac{\overrightarrow{B_n}\overrightarrow{r_{PQ}}}{R_{MP}}. \quad (6)$$

Although r_{PQ} may be different from an acquisition to another, the relative change is small due to the fact that the maximum measured LOS displacement must be smaller than $\lambda/2$ in order to avoid ambiguities. So the value used for the distance between the targets may be the one measured at the time prior to the master image acquisition.

3.1 Tracking simulation

In order to test the tracking procedure for practical situations, a set of simulations was realized using a deformation model provided by the EDF company regarding the Puylaurent dam [12]. Considering two stable scatterers placed on the ridge of the dam, the deformation model gives the unit vector $\overrightarrow{v}$ of the direction of relative movement. If this displacement is not orthogonal to the LOS direction (characterized by the unit vector $\overrightarrow{u_{LOS}}$), the actual displacement can be easily computed as:

$$D = \frac{D_{LOS}}{\overrightarrow{u_{LOS}}\overrightarrow{v}}. \quad (7)$$

In the simulations, different displacements were randomly generated (in keeping with real data) and the phase differences were computed for various positions of the satellite relative to the master position. The initial position vectors of the two targets were considered erroneous, which leads to a false first displacement. However, one displacement is relative to the previous one, so from the second image onwards the computed displacement is correct (the systematic error is cancelled). The simulation results are summarized in Fig. 2. By not taking into account the noise and atmospheric effects in the simulations, the very small absolute error is due to the approximations made in deriving Eq. 6.

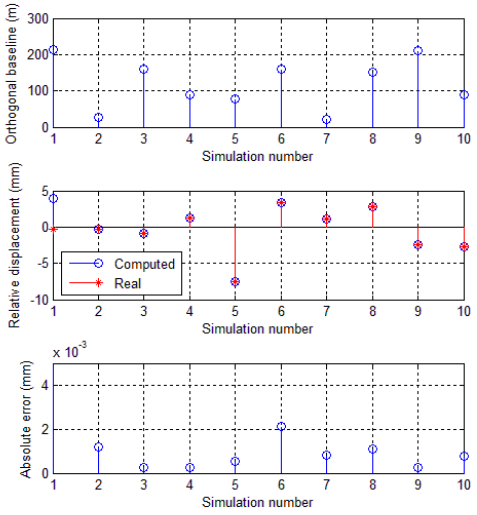

Figure 2: Puylaurent dam, France: tracking simulation results.

4 Results and discussion

In this section, a real data-set acquired by the TerraSAR-X satellite at X-band is analyzed: 4 stripmap (single polarization) images have been acquired over the "Chamonix Mont-Blanc" test site on 05, 16, 28 August and 21 October 2009. The best ground projected pixel spacing is respectively 2 m in azimuth and 2.2 m in range. Over the test site, two artificial targets (corner reflectors) have been installed in a geographical stable area (Refuge d'Argentière). Their initial location have been measured by differential GPS. One of the two targets has been manually moved before each acquisition using a fine-tunable support in the millimeter range and exact ground truth is available on the position and the displacement of the target.
Fig. 3 shows the parameter estimation results: (a) FP texture, (b) SCM normalized texture, (c) span, (d) trihedral target amplitude. The detection result obtained over the 05 August 2009 TerraSAR-X image is illustrated by the red triangles. In the left part of Fig. 3-(d) the two artificial corner reflectors are retrieved.
Finally, Fig. 4 illustrates the Line Of Sight (LOS) InSAR displacement error with respect to the "in situ" measure-

ments. In all cases, the fixed corner reflector was used to remove the atmospheric phase delay. The obtained overall accuracy is less than 0.75 mm displacement in LOS.

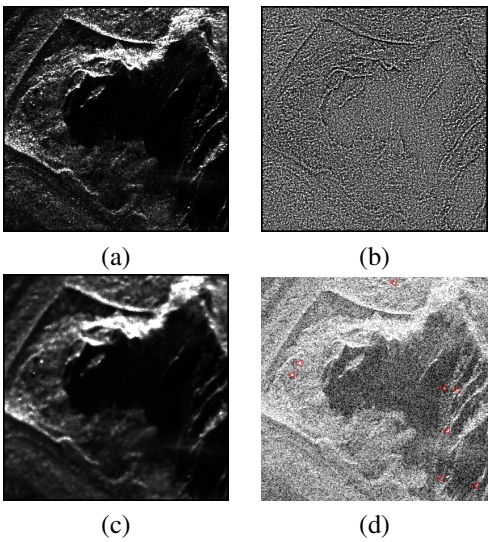

Figure 3: Refuge d'Argentière, TerraSAR-X data, 2009. (a) texture estimated using $\widehat{\tau}$, (b) normalized texture $\widehat{\xi}$, (c) span $\widehat{\sigma_0}$, and (d) detected SS using the 05 August 2009 image superposed over the target amplitude $\widehat{\alpha}$ from Eq. 4.

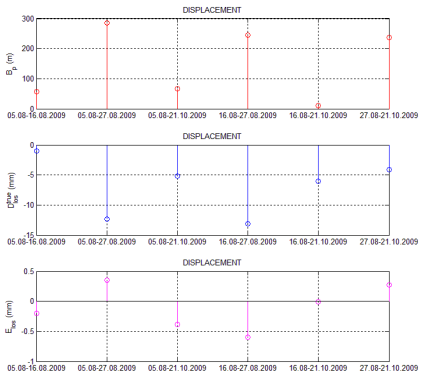

Figure 4: Refuge d'Argentière, TerraSAR-X data, 2009. (a) perpendicular interferometric baselines, (b) LOS "in situ" measured displacement, and (c) LOS interferometric displacement error.

5 Conclusions

A novel strategy for Stable Scatterers detection was introduced by coupling sub-band / sub-aperture decomposition prior to the GLRT-LQ detector. The tracking of slowly moving SS targets was preformed by repeat-pass SAR interferometry. A case study with TerraSAR-X data has been presented also. In the future, this technique will be applied for the Puylaurent dam monitoring over the year 2012.

Acknowledgment

The authors would like to thank the German Aerospace Center (DLR) for providing the high-resolution TerraSAR-X stripmap SAR images through the MTH0232 and MTH0828 projects. This work was supported by the Électricité de France (EDF) company.

References

[1] F. T. Ulaby, F. Kouyate, B. Brisco, and T. H. L. Williams, "Textural information in SAR images," *IEEE Transactions on Geoscience and Remote Sensing*, vol. GE-24, no. 2, pp. 235–245, 1986.

[2] R. Fjortoft and A. Lopes, "Estimation of the mean radar reflectivity from a finite number of correlated samples," *IEEE Transactions on Geoscience and Remote Sensing*, vol. 39, no. 1, pp. 196–199, 2001.

[3] M. S. Greco and F. Gini, "Statistical analysis of high-resolution SAR ground clutter data," *IEEE Transactions on Geoscience and Remote Sensing*, vol. 45, no. 3, pp. 566–575, 2007.

[4] G. Vasile, J.-P. Ovarlez, F. Pascal, M. Gay, G. d'Urso, and D. Boldo, "Stable scatterers detection and tracking in heterogeneous clutter by repeat-pass SAR interferometry," in *Proceedings of the Asilomar Conference on Signals, Systems, and Computers, Pacific Grove, California, USA*, 2010, pp. 1343–1347.

[5] A. Ferretti, C. Prati, and F. Rocca, "Permanent scaterrers in SAR interferometry," *IEEE Transactions on Geoscience and Remote Sensing*, vol. 39, no. 1, pp. 8–20, 2001.

[6] J.-P. Ovarlez, L. Vignaud, J.C. Castelli, M. Tria, and M. Benidir, "Analysis of SAR images by multidimensional wavelet transform," *IET Proc. Radar Sonar and Navigation*, vol. 150, no. 4, pp. 234–241, 2003.

[7] M. Duquenoy, J.-P. Ovarlez, L. Ferro-Famil, E. Pottier, and L. Vignaud, "Scatterers characterization in radar imaging using joint time-frequency analysis and polarimetric coherent decompositions," *IET Proc. Radar Sonar and Navigation*, vol. 4, no. 3, pp. 384–402, 2010.

[8] F. Pascal, Y. Chitour, J.-P. Ovarlez, P. Forster, and P. Larzabal, "Covariance structure maximum-likelihood estimates in compound Gaussian noise: existence and algorithm analysis," *IEEE Transactions on Signal Processing*, vol. 56, no. 1, pp. 34–48, 2008.

[9] E. Conte, M. Lops, and G. Ricci, "Asymptotically optimum radar detection in compound-Gaussian clutter," *IEEE Transactions on Aerospace and Electronic Systems*, vol. 31, no. 2, pp. 617–625, 1995.

[10] E. Jay, J.-P. Ovarlez, D. Declercq, and P. Duvaut, "BORD: Bayesian optimum radar detector," *Signal Processing*, vol. 83, no. 6, pp. 1151–1162, 2003.

[11] X. Ding, Z. W. Li, J. J. Zhu, G. Feng, and J.P. Long, "Atmospheric effects on InSAR measurements and their mitigation," *Sensors*, vol. 8, pp. 5426–5448, 2008.

[12] G. Geffray, "Rapport GEH Loire Ardeche : barrage de Puylaurent, auscultation juin 2006 - mai 2008," Tech. Rep. 6, EDF DTG, Grenoble, France, 2008.